Structural insights into GDP-mediated regulation of a bacterial acyl-CoA thioesterase

Received for publication, June 10, 2017, and in revised form, September 12, 2017 Published, Papers in Press, October 2, 2017, DOI 10.1074/jbc.M117.800227

Yogesh B. Khandokar[‡], Parul Srivastava[‡], Nathan Cowieson[§], Subir Sarker[¶], David Aragao[‖], Shubagata Das[**], Kate M. Smith[‡], Shane R. Raidal[**], and Jade K. Forwood[‡1]

From the [‡]School of Biomedical Sciences and [**]School of Animal and Veterinary Sciences, Charles Sturt University, Boorooma Street, Wagga Wagga, New South Wales 2678, Australia, the [§]Life Sciences Division, Diamond Light Source, Didcot OX11 0DE, United Kingdom, the [¶]Department of Physiology, Anatomy and Microbiology, School of Life Sciences, La Trobe University, Melbourne, Victoria 3086, Australia, and the [‖]Australian National Synchrotron, Melbourne, Victoria 3168, Australia

Edited by John M. Denu

Thioesterases catalyze the cleavage of thioester bonds within many activated fatty acids and acyl-CoA substrates. They are expressed ubiquitously in both prokaryotes and eukaryotes and are subdivided into 25 thioesterase families according to their catalytic active site, protein oligomerization, and substrate specificity. Although many of these enzyme families are well-characterized in terms of function and substrate specificity, regulation across most thioesterase families is poorly understood. Here, we characterized a TE6 thioesterase from the bacterium *Neisseria meningitidis*. Structural analysis with X-ray crystallographic diffraction data to 2.0-Å revealed that each protein subunit harbors a hot dog-fold and that the TE6 enzyme forms a hexamer with D3 symmetry. An assessment of thioesterase activity against a range of acyl-CoA substrates revealed the greatest activity against acetyl-CoA, and structure-guided mutagenesis of putative active site residues identified Asn^{24} and Asp^{39} as being essential for activity. Our structural analysis revealed that six GDP nucleotides bound the enzyme in close proximity to an intersubunit disulfide bond interactions that covalently link thioesterase domains in a double hot dog dimer. Structure-guided mutagenesis of residues within the GDP-binding pocket identified Arg^{93} as playing a key role in the nucleotide interaction and revealed that GDP is required for activity. All mutations were confirmed to be specific and not to have resulted from structural perturbations by X-ray crystallography. This is the first report of a bacterial GDP-regulated thioesterase and of covalent linkage of thioesterase domains through a disulfide bond, revealing structural similarities with ADP regulation in the human ACOT12 thioesterase.

Acyl-CoA thioesterases are a large family of enzymes that catalyze the hydrolysis of the thioester bond between a carbonyl group and a sulfur atom, producing fatty acids and CoA. These enzymes are conserved throughout evolution and are expressed ubiquitously in bacteria, fungi, plants, and mammals, and localized in a range of cellular organelles such as mitochondria, cytosol, endoplasmic reticulum, and peroxisomes (1). The structure and function of many thioesterases have been characterized recently from bacteria, plants, and animals (2–7), elucidating important roles in various lipid metabolic pathways through regulating the cellular concentrations of fatty acids, acyl-CoA, and CoASH (8, 9). The mechanistic details through which thioesterases carry out catalysis have also been described (10–18), utilizing either a two-step reaction mechanism involving nucleophilic attack by aspartate or glutamate to produce an enzyme–substrate intermediate (14, 17), or an alternative mechanism involving an acid/base-like catalytic reaction, where the carbonyl carbon atom is attacked directly by an aspartate-activated water molecule to cleave the thioester bond (17).

Although the structure, function, and catalytic reaction mechanisms are being unveiled for a range of thioesterase families, our knowledge of regulation within these enzyme families remains comparatively limited. In the human Them1 thioesterase, which hydrolyzes a range of fatty acyl-CoAs with preference for long chain acyl-CoA molecules, dimerization is induced by fatty acyl-CoAs, coenzyme A (CoASH), ATP, and ADP, and the catalytic activity enhanced by ATP and inhibited by ADP and CoA (19). In human ACOT12, a previous model of ADP and ATP regulation was proposed to be mediated through domain assembly but recently discounted with structural and biophysical evidence identifying a nucleotide-binding site located between two regulatory loop regions, one linking the hot dog domains, and the second involving the C terminus of the protein (4). Human ACOT9 has been shown to be negatively regulated by NADH and CoA, however, neither a structural nor biochemical basis for this regulation has been determined. Regulation of PaaI-type thioesterases revealed an induced fit regulatory mechanism and half-of-sites reactivity, with the binding of substrates inducing small rigid-body rearrangements of the hot dog domains that inhibit binding in two of four possible catalytic sites (10). Overall, these limited and varied snapshots of thioesterase regulation highlight the need for a greater understanding of how these enzymes are regulated to control the cellular concentrations of important metabolites including coenzyme A, and activated fatty acids.

The authors declare that they have no conflicts of interest with the contents of this article.

This article contains supplemental Fig. S1 and Tables S1 and S2.

The atomic coordinates and structure factors (codes 5V3A, 5SZZ, 5SZY, 5T02, and 5SZU) have been deposited in the Protein Data Bank (http://wwpdb.org/).

[1] To whom correspondence should be addressed: School of Biomedical Sciences, Wagga Wagga, NSW 2678, Australia. Tel.: 61-7-69332317; Fax: 61-7-69332587; E-mail: jforwood@csu.edu.au.

Table 1
Data collection and refinement statistics of *Nm*ACT-WT and mutants
Statistics for the highest-resolution shell are shown in parentheses.

Protein	*Nm*ACT-WT	*Nm*ACT-Cys^{158}-X	*Nm*ACT-N24A	*Nm*ACT-D39A	*Nm*ACT-Cys^{158}-X:R93E
Wavelength (Å)	0.9537	0.9786	0.9537	0.9537	0.9762
Resolution range (Å)	38.1–2.0 (2.1–2.0)	34.1–2.3 (2.4–2.3)	36.0–2.0 (2.1–2.0)	39.8–2.8 (2.9–2.8)	48.5–2.8 (2.9–2.8)
Space group	$P2_1$ 3	$P2_1$ 3	$P2_1$ 3	$P3_1$ 2 1	$P2_1$ 3
Unit cell	152.4 152.4 152.4	152.6 152.6 152.6	152.8 152.8 152.8	226.1 226.1 68.3 90 90 120	153.2 153.2 153.2
Unique reflections	79,515 (7,831)	52,676 (5,239)	80,089 (7,963)	49,406 (4,911)	28,972 (2,905)
Multiplicity	43 (42.0)	22 (21)	12 (12.2)	5.5 (4.8)	3.5 (3.4)
Completeness (%)	100.0 (100.0)	100.0 (100.0)	100.0 (100.0)	100.0 (100.0)	97.4 (99.7)
Mean $I/\sigma(I)$	18.4 (3.8)	40.4 (14.1)	23.6 (7.6)	13.9 (5.3)	6.5 (2.0)
Wilson *B*-factor	24.4	23.0	22.2	38.5	29.7
R_{merge}	0.029 (0.20)	0.013 (0.050)	0.020 (0.096)	0.041 (0.177)	0.123 (0.574)
Model refinement					
R_{work}	0.18 (0.22)	0.18 (0.20)	0.19 (0.22)	0.17 (0.23)	0.17 (0.25)
R_{free}	0.20 (0.24)	0.21 (0.27)	0.21 (0.22)	0.21 (0.27)	0.21 (0.32)
Refined model					
Atoms	5717	5363	5301	7407	4808
Water molecules	304	384	330	0	0
Molecules in ASU	4	4	4	6	4
Protein residues in ASU	616	592	588	901	588
R.m.s. deviation					
Bonds	0.009	0.016	0.008	0.009	0.017
Angles	1.75	1.76	1.43	1.26	1.57
Ramachandran					
Favored (%)	98	98	99	97	98
Allowed (%)	2	2	1	3	2
Outliers (%)	0	0	0	0	0
Average *B* factor (Å^2)	29.5	25.4	26.0	35.0	29.1
Macromolecules	29.9	25.0	25.7	35.1	29.2
Ligands	21.8	23.6	24.7	32.9	26.3
Solvent	30.9	31.7	30.8	N/A	N/A
PDB code	5V3A	5SZZ	5SZY	5T02	5SZU

Here, we provide structural insights into the regulation of an acyl-CoA thioesterase from *Neisseria meningitidis*. Through combined experimental approaches including X-ray crystallography, small-angle X-ray scattering, structure-guided mutagenesis, substrate specificity, and enzyme-activity assays, we have elucidated the binding pocket and regulatory allosteric effect of GDP. Importantly, the structural integrity of all mutants within the active site and GDP binding determinants did not perturb the structure of the enzyme. Overall, this study presents the first structural basis for GDP-mediated regulation within any thioesterase family, and identifies a possible evolutionary link with regulatory mechanisms identified in human thioesterases.

Results and discussion

Structure of NmACT

Fatty-acyl CoA thioesterases play essential roles in lipid metabolism and a wide range of cellular functions, however, regulation of these enzymes remains poorly understood across most thioesterase families. To better understand the structure, function, and regulation of a TE6 family member, we expressed and purified a thioesterase from *N. meningitidis* by affinity and size exclusion chromatography (supplemental Fig. S1), and characterized the enzyme by X-ray crystallography, substrate screening, enzyme kinetic assays, small angle X-ray scattering, and structure-guided mutagenesis.

Protein crystals grown in 100 mM Tris, pH 8.5, and 2 M ammonium phosphate, belongs to space group $P2_13$ diffracted to 2.0 Å at the Australian Synchrotron macromolecular crystallography beamlines, and the phases solved by molecular replacement using chain A from PDB[2] code 1VPM (33% sequence identity (20)) as a search model. Following model rebuilding and refinement in COOT (21) and Phenix (22), respectively, the final model consisted of residues 5–158, R_{work} and R_{free} values of 18 and 20%, respectively, and good stereochemistry (Table 1).

The crystal structure revealed each protomer within the enzyme contained a "hot dog"-fold, composed of a five-stranded anti-parallel β-sheet wrapping a central α-helix (Fig. 1*A*) (23, 24). The protein structure also revealed an additional C-terminal α-helix that packs against the β-sheet on the opposite side of the central α-helix (Fig. 1*A*). The overall topology of the protomer is $\beta1$-$\alpha1$-$\beta3$-$\beta4$-$\beta5$-$\alpha2$-$\beta2$ (Fig. 1*B*), with the β-strands varying in length from 8 to 16 amino acids, and the $\alpha1$ and $\alpha2$ helices composed of 22 and 21 residues, respectively.

The asymmetric unit (ASU) contained four protomers, all similar in structure with the greatest root mean square deviation (r.m.s. deviation) of 0.27 Å. The arrangement of these chains in the ASU (Fig. 2*A*) did not resemble the quaternary structure of any previously described thioesterase, and the contacts between the two hot dog dimers were unlikely to represent a stable biological unit. Examination of all possible oligomeric structures was assessed by characterizing the interfaces both within and outside of the asymmetric unit. Based on the extent of intermolecular interactions from this analysis, the most likely biological quaternary structure was a hexamer and

[2] The abbreviations used are: PDB, Protein Data Bank; ASU, asymmetric unit; r.m.s., root mean square; SAXS, small angle X-ray scattering.

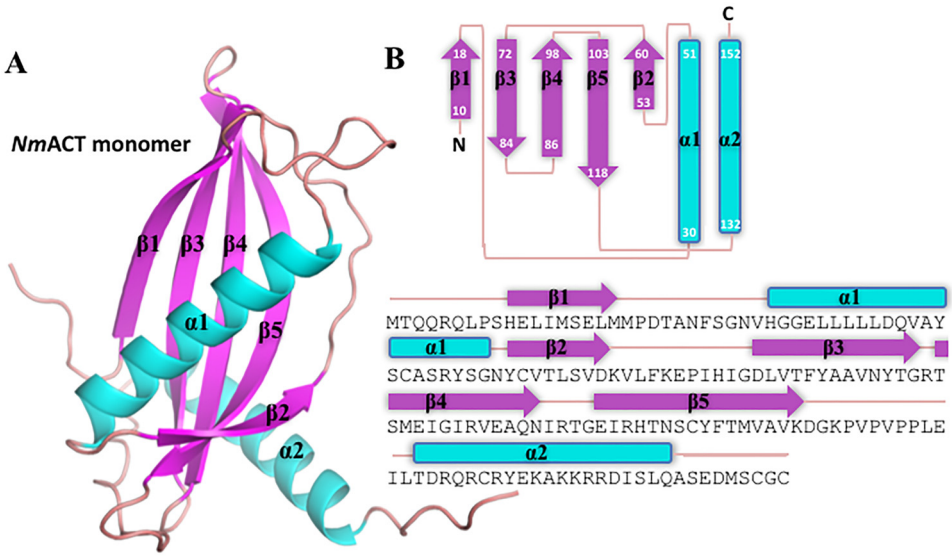

Figure 1. Structure of *Nm*ACT. *A,* each *Nm*ACT protomer contains a five-stranded β-sheet (*pink*) that wraps a central α-helix (*cyan*). An additional C-terminal α-helix packs against the β-sheet on the opposite side of the central α-helix. *B,* topology of *Nm*ACT and associated primary sequence.

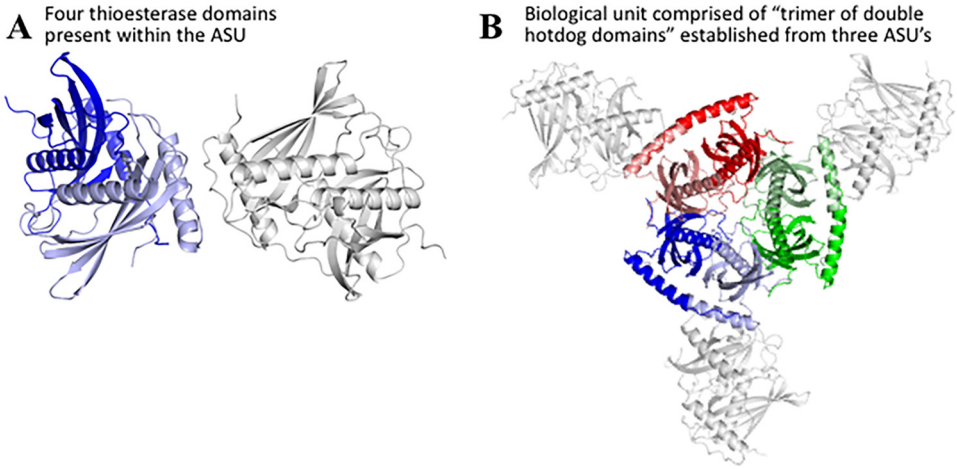

Figure 2. Quaternary structure of *Nm*ACT. *A,* the asymmetric unit is composed of four thioesterase arranged as double hot dog dimers. *B,* the biological unit, which is composed of a timer-of-double hot dog thioesterases, is formed from three asymmetric units.

formed from three ASU's each contributing two hot dog subunits (Fig. 2*B*). This is consistent with the structure analysis using the PDBe PISA server (25), the elution profile of the enzyme during size exclusion chromatography (supplemental Fig. S1) and biological assemblies obtained in different crystal forms (see Table 1). This proposed biological assembly also correlated well with small angle X-ray scattering data (Fig. 3), with the hexameric arrangement producing a χ^2 value of 0.83 (Table 2).

The biological assembly buries a total surface area of 18,878 Å^2, and two types of intermolecular interfaces contribute the majority of these interaction interfaces. The first type of interface is between two hot dog subunits creating a "double hot dog," with the two central α-helices arranged parallel (Fig. 4). This interface buries ~2,840 Å^2 of surface area, and is mediated by ionic interactions between His^{30}:Asp^{39} and Lys^{141}:Asp^{155}, and 10 hydrogen bonds (supplemental Table S1). The high resolution structure revealed two symmetry related disulfide interactions at the interface, involving Cys^{137} of one hot dog subunit, and Cys^{158} of the other hot dog subunit (Fig. 5). This is the first report of a disulfide bond bridging two hot dog subunits.

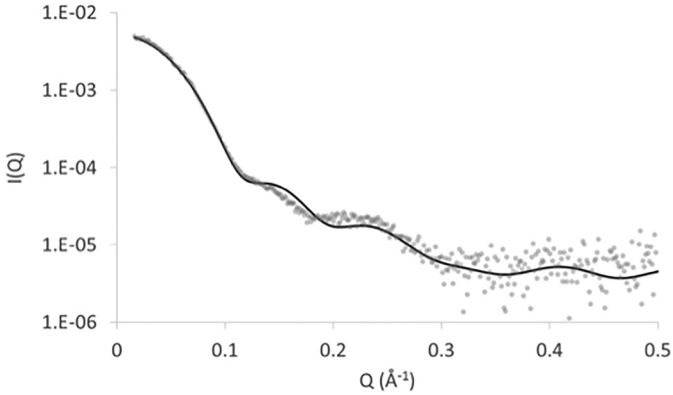

Figure 3. Small angle scattering profile of experimental data (*small gray dots*) and overlaid predicted scattering profile (*dark line*) of a hexameric thioesterase arranged with D3 symmetry as determined in the crystal structures.

Interestingly, we identified a GDP molecule bound at each disulfide bond (Fig. 5), also representing the first report of a GDP-bound thioesterase. Structural analysis revealed the GDP-binding pocket to be composed of Ala[78], Asn[81], Arg[93], Ser[109], Tyr[111], Arg[138], and Lys[141] from each hot dog protomer, Ser[157] and Cys[158] of another hot dog protomer within the double hot dog subunit, and Arg[5] from another hot dog subunit outside of the double hot dog subunit (Fig. 6).

In addition to the two GDP molecules bound at each hot dog dimer interface, each dimer also contained two bound CoA molecules, positioned with the terminal sulfur in close proximity to putative active site residues Asn[24] and Asp[39]. Each CoA makes H-bond interactions with Thr[56], Phe[64], Lys[65], Arg[85], Thr[86], Ser[87], Arg[146], and Ser[149] (supplemental Table S2).

The second of the two major interfaces involve two hot dog domains associating through β-strand one, the central α-helices, and various loop regions (Fig. 4). Each interaction interface buries 2,650 Å^2, and the interface is mediated by salt bridge interactions involving Arg[5] and Glu[95], and 8 hydrogen bonds (supplemental Table S1).

Table 2
SAXS data statistics

Data collection parameters	
Instrument	Australian Synchrotron SAXS/WAXS beamline
Beam geometry	120-μm point source
Wavelength	1.033 (Å)
Q range	0.009 to 0.54 Å^{-1}
Exposure time	18 × 1 s exposures
Sample flow	4 ml/s
Concentration range	0.07–1.1 mg/ml
Temperature	283 K
Structural parameters	
$I(0)$ (from P(r))	5.45E-03 cm^{-1}
R_g (from P(r))	30.08 (Å)
$I(0)$ (from Guinier)	5.41E-03 (cm^{-1})
D_{max}	81 (Å)
R_g (from Guinier)	30.63 (Å)
Porod volume estimate	167,974 (Å^{-3})
Dry volume calculated from sequence	127,128 (Å^{-3})
Molecular mass determination	
Partial specific volume	0.736 (cm^3 g^{-1})
Contrast	2.897 ($\Delta\rho \times 10^{10}$ cm^{-2})
Molecular mass M_r (from I(0))	102.1 kDa
Protomer 103.8 (hexamer)	M_r from sequence, 17.3 (protomer)
Software employed	
Primary data reduction	ScatterBrain (Australian Synchrotron)
Model intensities computation	CRYSOL
Graphics representations	PyMOL

Enzyme activity and substrate specificity

Because the specificity of the enzyme has not been determined previously, we screened a range of substrates using an established 5,5′-dithiobis(nitrobenzoic acid) assay (26, 27) to identify the substrate specificity. Substrates ranging in carbon chain length from two (C2) to 20 (C20) were screened, with the highest activity observed for acetyl-CoA (Fig. 7); K_m = 2.1 mM and K_{cat} = 33 s^{-1} (Table 3). Catalytic residues within thioesterases vary considerably across different family members (4, 20, 26–29), therefore to establish residues involved in *Nm*ACT activity, putative catalytic residues in close proximity to the terminal sulfur atom in CoA were mutated, and the proteins were assessed for activity. Residues Asn[24] and Asp[39] were mutated to Ala residues and tested for activity against acetyl-CoA. Both *Nm*ACT-N24A and *Nm*ACT-D39A variants displayed negligible thioesterase activity (Fig. 7), implying these residues are important for catalysis. To confirm that the mutations do not perturb the structural integrity of the proteins, the elution profiles of the mutant enzymes were shown to be identical to that of the wild-type enzyme and the structures were confirmed by crystallography. Both *Nm*ACT-N24A and *Nm*ACT-D39A exhibited the same structures, including subunit and biological assemblies as the wild-type enzyme (r.m.s.

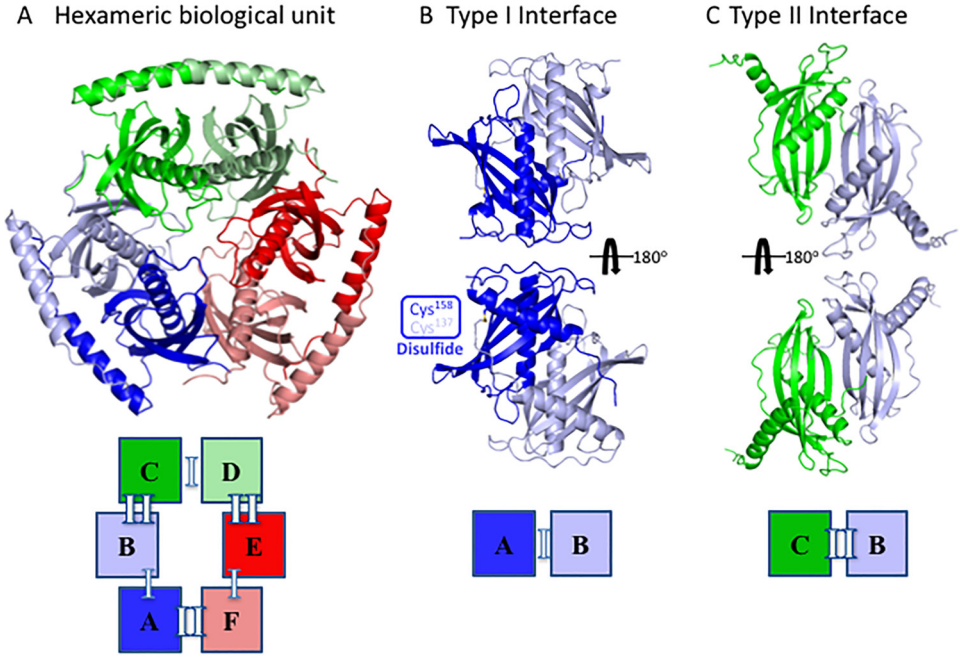

Figure 4. The biological unit of the *Nm*ACT is composed of a hexamer of thioesterase domain protomers exhibiting D3 symmetry (*left*). The two interfaces that mediate arrangement of the biological assembly are depicted *middle* and *right panels*.

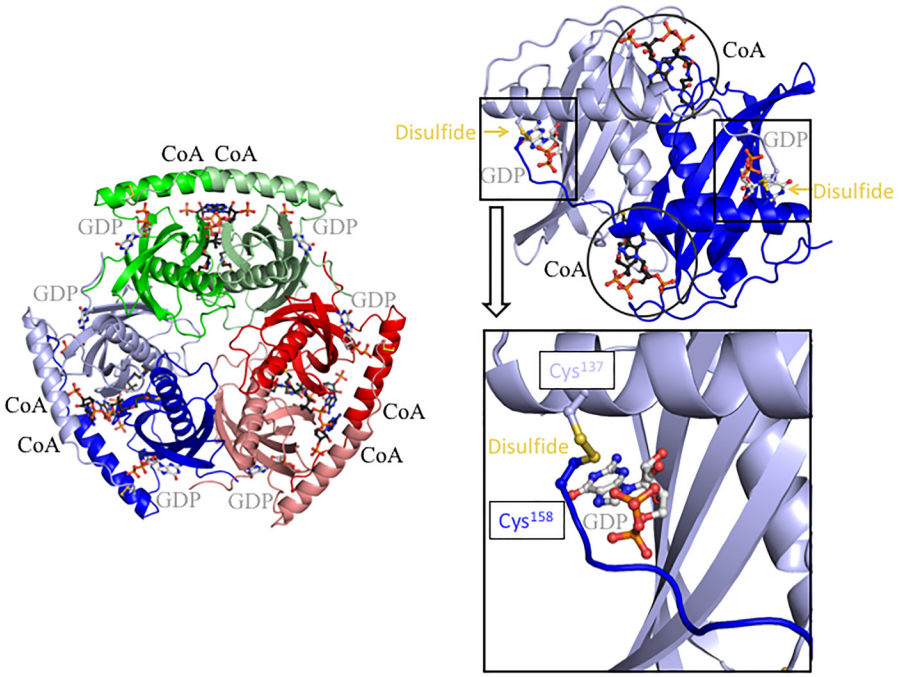

Figure 5. Each biological unit contained six GDP molecules, six CoA molecules, and six disulfide bonds. Both the molecules and disulfide bonds are from interactions across thioesterase protomers in a double hot dog configuration.

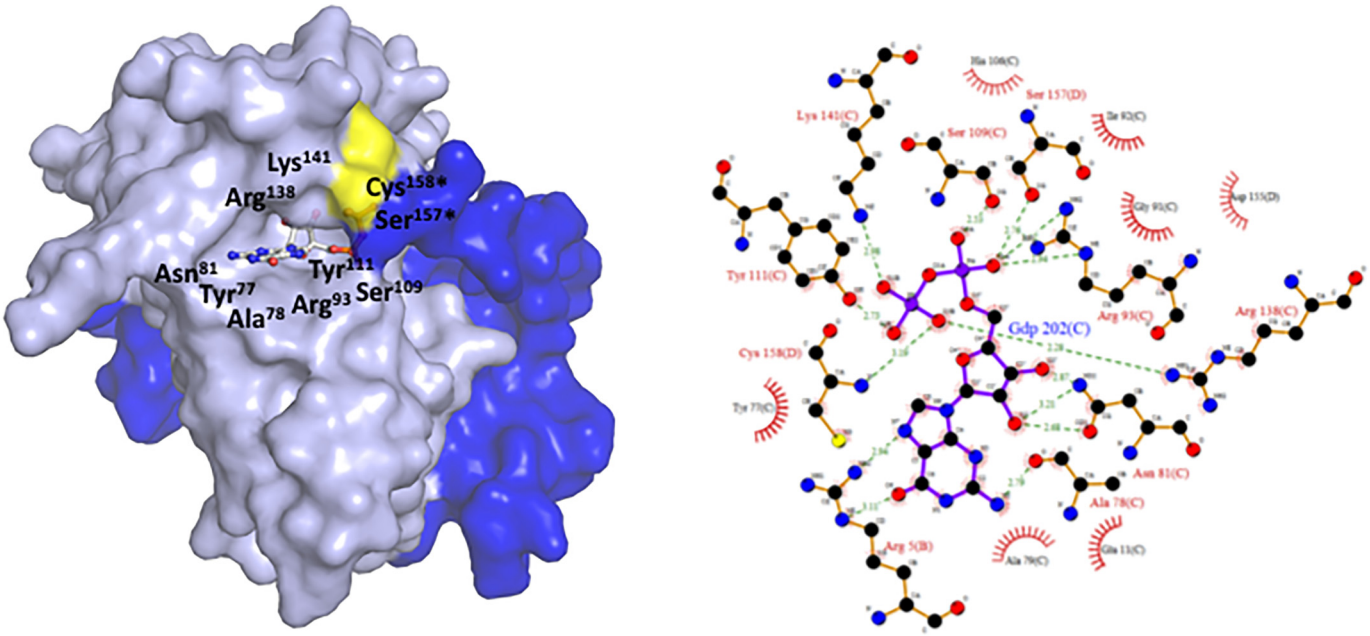

Figure 6. Surface view of a double hot dog domain and bound GDP. *Left*, residues that contribute the binding pocket are depicted. *Right*, detailed bonding interactions of GDP using Ligplot. Hydrogen bonds are depicted as *green dashes*, and hydrophobic interactions as *red fans*.

deviation <0.50). These active site residues appear to be conserved across a wide range of thioesterase proteins (Fig. 8).

Assessing the role of the Cys^{137}:Cys^{158} disulfide bond and GDP

The presence of a disulfide bond that covalently tethers two hot dog domains in a double hot dog configuration has not been observed previously. The covalent linkage of thioesterase domains is a distinguishing feature between prokaryotic and eukaryotic thioesterases, with prokaryotic thioesterases generally encoding single thioesterase domain proteins, whereas eukaryotic thioesterases harbor fused thioesterase domains (Fig. 9). Therefore, the covalent linkage of thioesterase domains within a double hot dog domain was unexpected, and since GDP was also found to be in close proximity to the disulfide bond, we tested whether disruption of the disulfide interaction and GDP binding may affect activity. Each disulfide bond is composed of Cys^{137} from one hot dog chain, and Cys^{158} of another within the hot dog dimer across the type 1 interface, and since the three residues at the C terminus of the enzyme contained Cys^{158}, Gly^{159}, and Cys^{160}, we introduced a stop

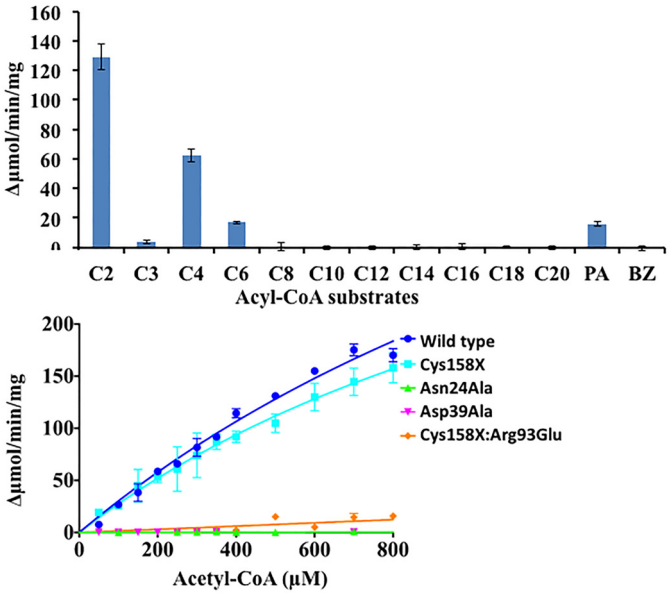

Figure 7. Activity of *Nm*ACT and mutants against acetyl-CoA substrate. *Upper panel*, screening of substrates (330 μM of each substrate per reaction, acetyl-CoA (C2-CoA), malonyl-CoA (C3-CoA), butyryl-CoA (C4-CoA), hexanoyl-CoA (C6-CoA), octanoyl-CoA (C8-CoA), decanoyl-CoA (C10-CoA), lauroyl-CoA (C12-CoA), myristoyl-CoA (C14-CoA), palmitoyl-CoA (C16-CoA), stearoyl-CoA (C18-CoA), and arachidonoyl-CoA (C20-CoA)) against *Nm*ACT. *Lower panel*, specific activity comparison of *Nm*ACT and mutants including *Nm*ACT-Cys^{158}-X, *Nm*ACT-N24A, *Nm*ACT-D39A, and *Nm*ACT-Cys^{158}-X:R93E.

Table 3

Kinetic parameters of *Nm*ACT-WT and variants

Enzyme	K_m	K_{cat}	K_{cat}/K_m
	mM	s^{-1}	$M^{-1}s^{-1}$
*Nm*ACT-WT	2.1 ± 0.5	33 ± 6	15.6×10^{-3}
*Nm*ACT-Cys^{158}-X	1.6 ± 0.5	24 ± 6	14.4×10^{-3}
*Nm*ACT-N24A	ND[a]	ND	ND
*Nm*ACT-D39A	ND	ND	ND
*Nm*ACT-Cys^{158}-X:R93E	ND	ND	ND

[a] ND stands for not determined due to low activity.

codon at Cys^{158} (*Nm*ACT-Cys^{158}-X) to ensure complete abrogation of any disulfide formation, and preventing the possibility of Cys^{160} forming a disulfide bond. The *Nm*ACT-Cys^{158}-X mutant protein was expressed successfully and eluted from the size exclusion column with a profile similar to that of the wild-type enzyme, indicating that the quaternary structure was also maintained. Additionally, we crystallized *Nm*ACT-Cys^{158}-X to examine whether any local differences were present (structural comparisons of mutants presented below). The overall structure was found to be highly similar to that the of wild-type enzyme, with an overall r.m.s. deviation of 0.29 Å. Notably, the C-terminal residues ^{153}SEDMSC could not be modeled in *Nm*ACT-Cys^{158}-X due to poor electron density, indicating a higher degree of flexibility in this region, however, the overall position of the C-terminal helices remained identical. We also noted a minor change in the β-bulge, particularly at Lys^{61}, which shifts 2.2 Å. Given these minimal local changes, we tested whether these could have an effect on enzyme activity. We found no significant difference in the enzyme activity of *Nm*ACT-Cys^{158}-X (Fig. 7; see Table 3; K_m 1.6 mM, K_{cat} 24 s^{-1}), indicating that the disulfide bond does not appear to play a role for activity. This is not unexpected because the covalent fusion of hot dog domains in eukaryotic thioesterases also appears to be not essential for activity (29). It therefore remains unclear from an enzyme catalytic perspective, why some hot dog domains are fused, particularly eukaryotic thioesterases, whereas others can form the same oligomeric biological unit and carry out the same reactions from a single thioesterase domain.

The elucidation of a bound GDP molecule orientated with the terminal β-phosphate moiety toward the disulfide bond, suggested a possible role in regulation. Because the GDP co-purified with the enzyme, and high ionic strength buffers, pH trials, and denaturants failed to dissociate the nucleotide, to test the importance of GDP binding on activity, we designed a structure-guided mutation in the GDP-binding pocket to disrupt binding, and assessed for activity against acetyl-CoA. Because the residues that mediate disulfide bond formation also contribute to GDP binding, we examined whether GDP was present in the crystals of *Nm*ACT-Cys^{158}-X. Strong density corresponding to GDP was observed (Fig. 10), indicating that this mutation alone was not sufficient to disrupt GDP binding. We therefore used the *Nm*ACT-Cys^{158}-X mutant to create additional, structure-guided mutants to disrupt the GDP interaction. We found that whereas the *Nm*ACT-Cys^{158}-X contained GDP in the crystal structure, an *Nm*ACT-Cys^{158}-X:R93E mutation displaced GDP from the binding pocket (Fig. 10). This establishes Arg^{93} as an important binding determinant in the interaction, and is consistent with the structure analysis identifying ionic interactions between the α-phosphate group of GDP and the positively charged Arg guanidinium group (Fig. 6). Significantly, the overall structure of the *Nm*ACT-Cys^{158}-X:R93E mutant was almost identical to that of *Nm*ACT-Cys^{158}-X, and exhibited a similar elution profile during size exclusion chromatography. We found a significant decrease in the activity of the *Nm*ACT-Cys^{158}-X:R93E variant compared with both wild-type and *Nm*ACT-Cys^{158}-X (Fig. 7), suggesting GDP may be important for activity. This is the first report of a thioesterase requiring GDP for activity. Other thioesterases regulated by nucleotides include ACOT11 (Them1), containing dual hot dog domains and a steroidogenic acute regulatory protein-related lipid transfer (START) domain, where dimerization can be induced by both ATP and ADP (19). ACOT12 has shown to be regulated by nucleotide-induced changes but through a different mechanism. The structure of ACOT12 revealed the oligomeric state is unaltered in the absence or presence of ADP, with ACOT12 exhibiting a trimer of double hot dog domain protomers, similar to all TE6 thioesterases. Rather than alteration of the oligomeric state of the enzyme, the regulatory mechanism of regulation was shown to occur through two regulatory regions (4). That GDP activates related hydrolases has been reported for the heterodimeric RagA/B–C/D complex, responsible for regulating the rapamycin complex 1. Here, GDP-bound RagC/D binds Raptor, leading to activation of TORC1 (30).

Structure comparison of wild-type NmACT and variants

The structures of the *Nm*ACT wild-type, active site variant *Nm*ACT-N24A, disulfide variant *Nm*ACT-Cys^{158}-X, and GDP-binding site variant *Nm*ACT-Cys^{158}-X:R93E were solved in the same space group ($P2_13$). One variant that readily pro-

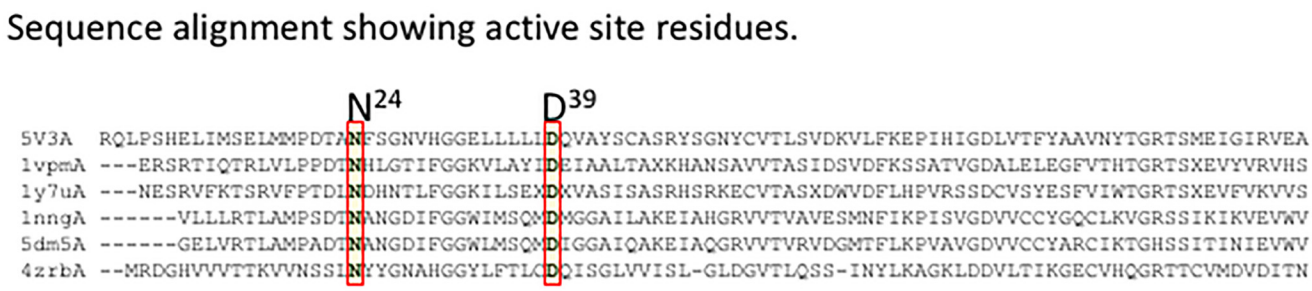

Figure 8. Structural alignment of thioesterases deposited to the PDB. The Asn[24] and Asp[39] residues, identified as catalytically important, are highly conserved.

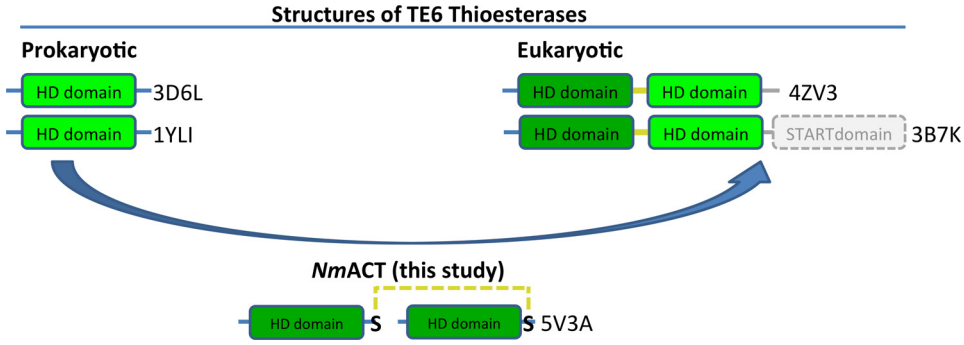

Figure 9. Domain organization of TE6 thioesterases. Prokaryotic thioesterases harbor single thioesterase domains, whereas eukaryotic ones contain fused thioesterase domains. The linkage of thioesterase domains by a disulfide bond may be analogous to a double hot dog domain fusion observed in eukaryotes.

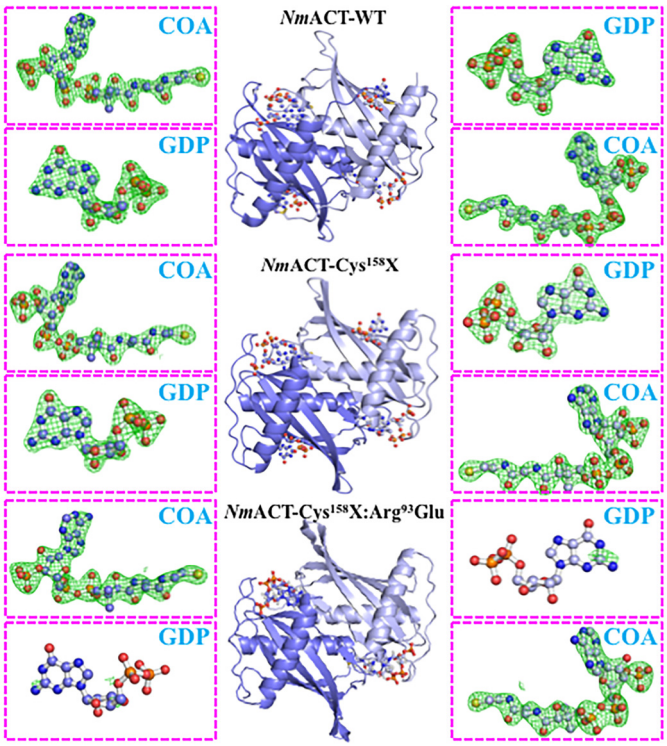

Figure 10. Dimer of (*A*) *Nm*ACT-WT and (*B*) truncated version *Nm*ACT-Cys[158]-X showing the presence of CoA and GDP supported by a $2F_o - F_c$ annealed omit map contoured at 2σ (*green mesh*), whereas (*C*) Cys[158]-X:R93E has no GDP supported, by an absence of density from a $2F_o - F_c$ annealed omit map contoured at 2σ (*green mesh*).

duced crystals in a different space group was the active site mutant *Nm*ACT-D39A, crystallizing in $P3_121$. Details of all data collections and refinement statistics of structures are presented in Table 1. The structural alignment of variants *Nm*ACT-Cys[158]-X, *Nm*ACT-N24A, *Nm*ACT-D39A, and *Nm*ACT-Cys[158]-X:R93E with *Nm*ACT-WT showed high similarity (Fig. 11) in the quaternary structure with r.m.s. deviation values of 0.29, 0.48, 0.50, and 0.57 Å, respectively. We also ensured the elution profiles from analytical size exclusion experiments were identical between wild-type and all variants, which together with crystallography data, ensure that the observed differences in activity are specific rather than the result of perturbations in enzyme structure and/or oligomerization.

Comparison of NmACT with human ACOT12

This is the first report and structural characterization of a prokaryotic thioesterase bound with GDP. One other structure deposited to the PDB has been used to describe nucleotide-binding and regulation, and this was for the multidomain human thioesterase, ACOT12 (4). Although the domain organization in ACOT12, which contains two non-identical hot dog domains and a C-terminal steroidogenic acute regulatory protein-related lipid transfer (START) domain, is markedly different to *Nm*ACT, the structural assembly of the thioesterase domains are surprisingly similar (Fig. 12). Notably, in the ACOT12 structure, only three coenzyme A and ADP molecules are present from a possible six sites, which is likely due to the eukaryotic thioesterase containing two fused, non-identical hot dog domains. In contrast, *Nm*ACT, which harbors six identical domains in the biological unit, has six GDP and coenzyme A molecules bound at all symmetry related sites (Fig. 12). To test if the location of the coenzyme A and regulatory nucleotide molecules were conserved, the structures of *Nm*ACT and ACOT12 were superimposed. We found that both coenzyme A and nucleotide molecules were positioned and orientated in almost identical fashion in both bacterial and human thioes-

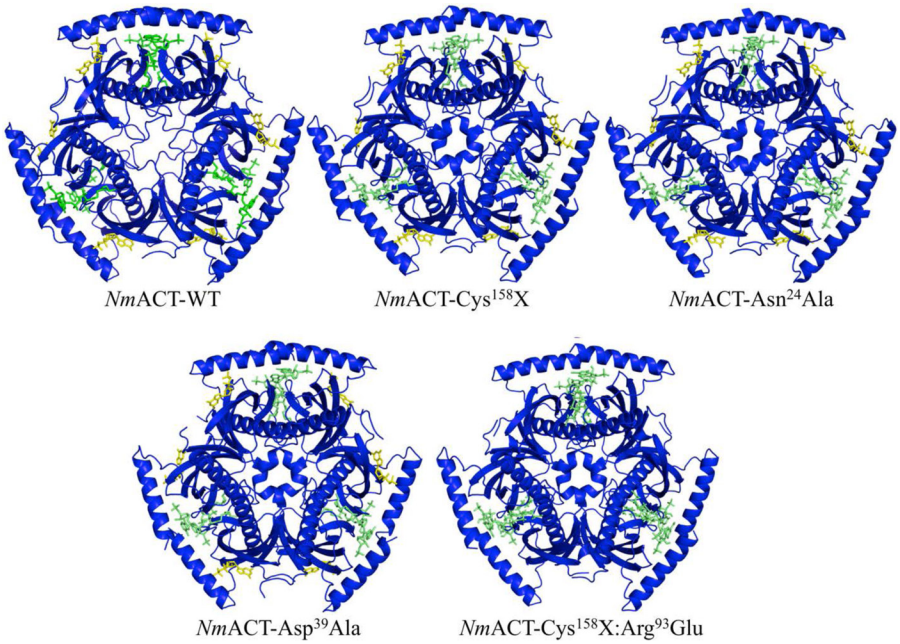

Figure 11. **Quaternary structures of *Nm*ACT wild-type, truncated mutant (Cys[158]-X), and mutants targeting the active site (N24A and D39A) and GDP binding (Cys[158]-X:R39E) confirming similar structures and mutations do not disrupt the structure.**

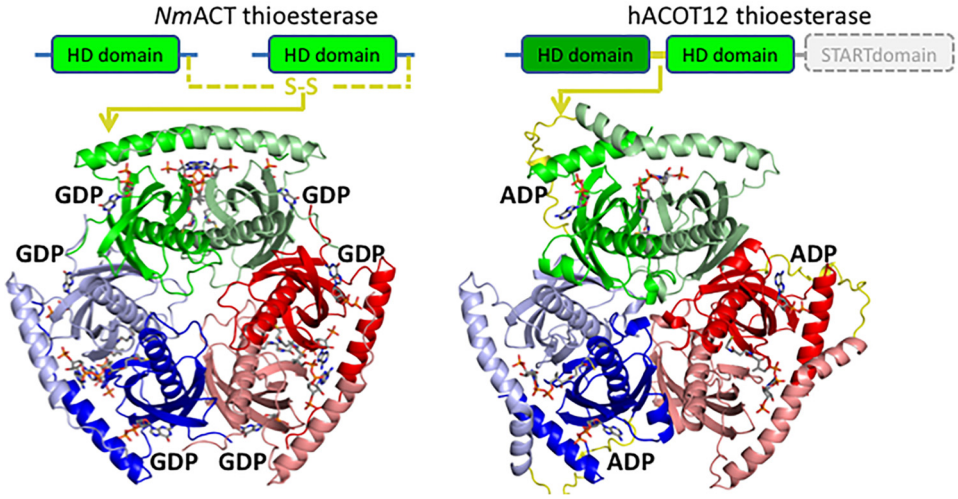

Figure 12. Structural comparison of *Nm*ACT and hACOT12. The overall arrangement of thioesterase domains is highly similar. *Nm*ACT binds six GDP and six CoA molecules, whereas hACOT12 binds only half the number due to non-identical hot dog domains. Fusion of the thioesterase domains have arisen through domain duplication, whereas *Nm*ACT has fused double hot dog dimers through a disulfide linkage.

terases (Fig. 13 and 14). Significantly, residues important for mediating H-bond interactions in the ACOT12-ADP structure, Asn[252], Arg[264], Ser[283], Arg[312], and Arg[313], were highly conserved in the *Nm*ACT structure (Fig. 14). Although the similar position and orientation of the bound nucleotides in *Nm*ACT and ACOT12 is indicative of a conserved regulatory mechanism, there are notable differences between the two structures, which likely reflects the mechanism through which the two thioesterase domains are bound. In ACOT12, nucleotide regulation was reported to occur through the linker region between the two hot dog domains (residues 154–178), and the C-terminal hot dog domain (4). Interestingly, because *Nm*ACT is a single thioesterase domain, it lacks an equivalent linker region. In this case, the hot dog domains are instead covalently linked through a disulfide interaction, which interacts with the nucleotide, however, we have shown that this disulfide interaction is not strictly required for GDP-mediate regulation. Thus, both prokaryotic and eukaryotic thioesterases display nucleotide-mediated regulation but through different mechanisms, as well as contrasting methods of tethering double hot dog domains.

Conclusion

This study describes a unique fusion of hot dog domain dimers mediated by disulfide bonds, present within a hexameric thioesterase. A GDP molecule was found positioned at each of these disulfide interaction sites and through structure guided-mutational analysis, we identified Arg[93] as an important binding determinant. The R93D mutation prevented GDP binding, and abolished enzyme activity, whereas retaining the

same tertiary and quaternary structural features as the wild-type enzyme (confirmed by X-ray crystallography). This established a clear link between GDP binding and enzyme activity, not described previously in any other thioesterase to date. Mutational analysis of putative active site residues identified Asn[24] and Asp[39] as important for catalysis, and these catalytic residues are conserved across many thioesterases. Finally, structural comparisons with the recently elucidated human thioesterase, ACOT12, revealed structural similarities in nucleotide binding. Overall, our study reveal high resolution structural insights into nucleotide binding within thioesterases, which are important for enzyme activity.

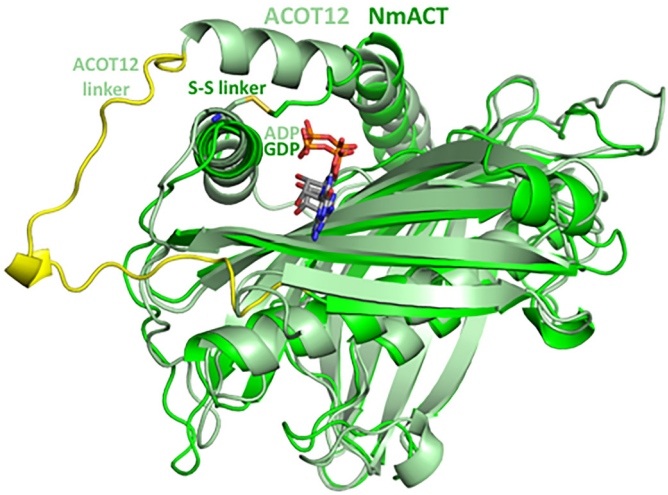

Figure 13. Superimposition of a double hot dog dimer of *Nm*ACT with a protomer of hACOT12. Shown are the GDP and ADP nucleotides superimposed and positioned in highly similar orientations.

Experimental procedures

Expression, purification, and crystallization

The expression, purification and crystallization of *Nm*ACT-WT, *Nm*ACT-Cys[158]-X, *Nm*ACT-N24A, *Nm*ACT-D39A, and *Nm*ACT-Cys[158]-X:R93E were carried out as described in our crystallization report (7). All constructs were co-crystallized with CoA in multiple crystallizing conditions as reported for *Nm*ACT-WT (7). Crystals grown in 100 mM Tris, pH 8.5, and 2 M ammonium phosphate led to complete datasets for *Nm*ACT-WT, *Nm*ACT-Cys[158]-X, *Nm*ACT-N24A, *Nm*ACT-D39A, and *Nm*ACT-Cys[158]-X:R93E, and diffraction to 2.0, 2.3, 2.0, 2.8, and 2.8Å, respectively. Crystals of *Nm*ACT-D39A were grown in 0.4 M ammonium phosphate monobasic and diffracted to 2.8 Å.

Crystal structure determination

Sparse matrix screening was performed using the hanging drop vapor diffusion method and a 1:1 ratio of protein:reservoir solution. Positive conditions were optimized by varying pH and

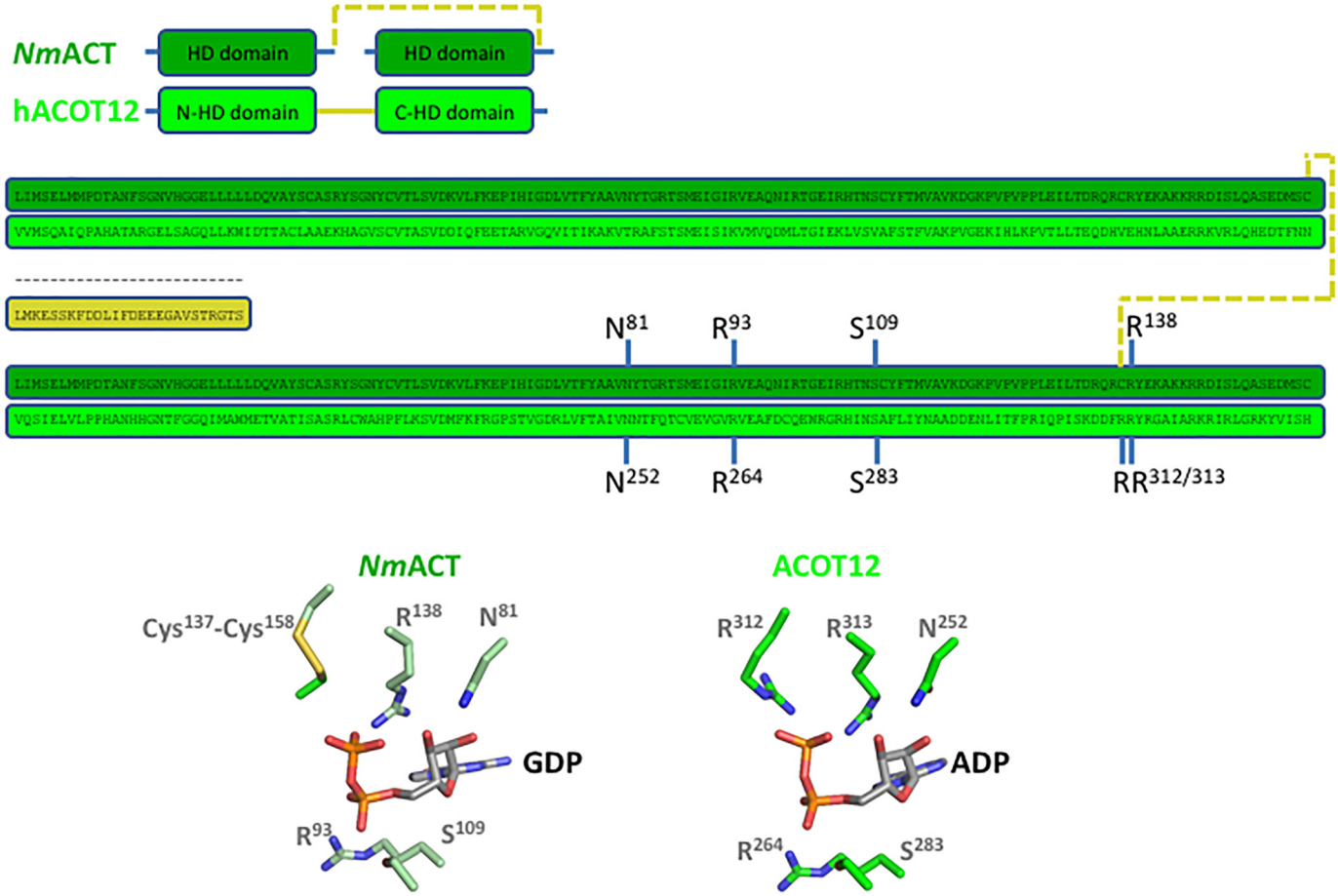

Figure 14. The nucleotide-binding residues in ACOT12 are highly similar in *Nm*ACT. *Nm*ACT contains single thioesterase domains fused as a double hot dog dimer through a disulfide interaction, whereas ACOT12 is fused through a 26-amino acid linker.

concentrations of precipitant and protein. Crystals were diffracted at the Australian Synchrotron, and reflections indexed, integrated, scaled, and merged in *i*MOSFLM and AIMLESS (31). Phases were determined by molecular replacement using *Bacillus halodurans* PDB code 1VPM (33% identity) as a search model for *Nm*ACT wild-type (*Nm*ACT-WT) and the latter to determine structures of *Nm*ACT mutants. Model building and refinement were performed using COOT (21) and Phenix (22), producing models with R/R_{free} of 0.17–0.19 and 0.20–0.21, respectively. The structures have been deposited to the PDB and issued codes 5V3A, 5SZZ, 5S2Y, 5T02, and 5SZU.

Substrate specificity assay

*Nm*ACT substrate specificity was determined spectrophotometrically at 412 nm against a wide range of commercially available acyl-CoA substrates. The enzymatic activity was recorded as the increase in the formation of 2-nitro-5-thiobenzoate anion (TNB^{2-}), a chromogenic substrate that can be measured at 412 nm (ϵ = 13,600 M^{-1} cm^{-1}) by the reaction of 5,5′-dithiobis(nitrobenzoic acid) with free CoASH (27). Reactions were started by the addition of substrate, and the absorption at 412 nm followed for 20 min at 25 °C over a range of substrate concentrations. The calculation of specific activity of the enzyme was done using Prism software, where the readings of two independent experiments performed in triplicate were used. The enzyme specific activity is expressed in mmol/min/mg.

Small angle X-ray scattering (SAXS)

Data were collected at the Australian Synchrotron on the SAXS/WAXS beamline using the Pilatus 1M detector. Data were collected over concentration ranges of 0.07–1 mg/ml. For each sample, 50 μl of sample was drawn through a 1.5-mm quartz capillary and exposed to the X-ray beam while moving. To control for radiation damage, 18 × 1-s exposures were made and compared for evidence of systematic change. The scattering data were collected at 10 °C with a beam energy of 11 KeV and in a Q range from 0.009 to 0.541 $Å^{-1}$, multiple images were averaged together and background subtracted. Detector images for each concentration were averaged using Scatterbrain to generate a number of SAXS data sets for subsequent analysis using ATSAS (version 2.4.3) software (32). PRIMUS was used to subtract background scattering from data files and Guinier fits and P(r) distribution plots were generated using GNOM. CRYSOL was used to generate theoretical curves and compare scattering data with crystal structure data.

Author contributions—Y. K. participated in the research. Y. B. K., P. S., N. C., S. S., D. A., S. D., K. M. S., S. R. R., and J. K. F. participated in writing and editing the final manuscript.

References

1. Kirkby, B., Roman, N., Kobe, B., Kellie, S., and Forwood, J. K. (2010) Functional and structural properties of mammalian acyl-coenzyme A thioesterases. *Prog. Lipid Res.* **49,** 366–377
2. Kotowska, M., and Pawlik, K. (2014) Roles of type II thioesterases and their application for secondary metabolite yield improvement. *Appl. Microbiol. Biotechnol.* **98,** 7735–7746
3. Rodríguez-Rodríguez, M. F., Salas, J. J., Garcés, R., and Martínez-Force, E. (2014) Acyl-ACP thioesterases from *Camelina sativa*: cloning, enzymatic characterization and implication in seed oil fatty acid composition. *Phytochemistry* **107,** 7–15
4. Swarbrick, C. M., Roman, N., Cowieson, N., Patterson, E. I., Nanson, J., Siponen, M. I., Berglund, H., Lehtiö, L., and Forwood, J. K. (2014) Structural basis for regulation of the human acetyl-CoA thioesterase 12 and interactions with the steroidogenic acute regulatory protein-related lipid transfer (START) domain. *J. Biol. Chem.* **289,** 24263–24274
5. Park, H., Graef, G., Xu, Y., Tenopir, P., and Clemente, T. E. (2014) Stacking of a stearoyl-ACP thioesterase with a dual-silenced palmitoyl-ACP thioesterase and 12 fatty acid desaturase in transgenic soybean. *Plant Biotechnol. J.* **12,** 1035–1043
6. Wu, R., Latham, J. A., Chen, D., Farelli, J., Zhao, H., Matthews, K., Allen, K. N., and Dunaway-Mariano, D. (2014) Structure and catalysis in the *Escherichia coli* hotdog-fold thioesterase paralogs YdiI and YbdB. *Biochemistry* **53,** 4788–4805
7. Khandokar, Y. B., Londhe, A., Patil, S., and Forwood, J. K. (2013) Expression, purification and crystallization of acetyl-CoA hydrolase from *Neisseria meningitidis*. *Acta Crystallogr. Sect. F Struct. Biol. Cryst. Commun.* **69,** 1303–1306
8. Hunt, M. C., Siponen, M. I., and Alexson, S. E. (2012) The emerging role of acyl-CoA thioesterases and acyltransferases in regulating peroxisomal lipid metabolism. *Biochim. Biophys. Acta* **1822,** 1397–1410
9. Hunt, M. C., and Alexson, S. E. (2002) The role Acyl-CoA thioesterases play in mediating intracellular lipid metabolism. *Prog. Lipid Res.* **41,** 99–130
10. Kunishima, N., Asada, Y., Sugahara, M., Ishijima, J., Nodake, Y., Sugahara, M., Miyano, M., Kuramitsu, S., Yokoyama, S., and Sugahara, M. (2005) A novel induced-fit reaction mechanism of asymmetric hot dog thioesterase PAAI. *J. Mol. Biol.* **352,** 212–228
11. Angelini, A., Cendron, L., Goncalves, S., Zanotti, G., and Terradot, L. (2008) Structural and enzymatic characterization of HP0496, a YbgC thioesterase from *Helicobacter pylori*. *Proteins* **72,** 1212–1221
12. Koglin, A., Löhr, F., Bernhard, F., Rogov, V. V., Frueh, D. P., Strieter, E. R., Mofid, M. R., Güntert, P., Wagner, G., Walsh, C. T., Marahiel, M. A., and Dötsch, V. (2008) When the fold fits the function: the external thioesterase of the surfactin-synthetase. *Nature* **454,** 907–911
13. Willis, M. A., Zhuang, Z., Song, F., Howard, A., Dunaway-Mariano, D., and Herzberg, O. (2008) Structure of YciA from *Haemophilus influenzae* (HI0827), a hexameric broad specificity acyl-coenzyme A thioesterase. *Biochemistry* **47,** 2797–2805
14. Cao, J., Xu, H., Zhao, H., Gong, W., and Dunaway-Mariano, D. (2009) The mechanisms of human hotdog-fold thioesterase 2 (hTHEM2) substrate recognition and catalysis illuminated by a structure and function based analysis. *Biochemistry* **48,** 1293–1304
15. Weeks, A. M., and Chang, M. C. (2012) Catalytic control of enzymatic fluorine specificity. *Proc. Natl. Acad. Sci. U.S.A.* **109,** 19667–19672
16. Labonte, J. W., and Townsend, C. A. (2013) Active site comparisons and catalytic mechanisms of the hot dog superfamily. *Chem. Rev.* **113,** 2182–2204
17. Cantu, D. C., Ardèvol, A., Rovira, C., and Reilly, P. J. (2014) Molecular mechanism of a hotdog-fold acyl-CoA thioesterase. *Chemistry* **20,** 9045–9051
18. Rabbani, N., Xue, M., and Thornalley, P. J. (2014) Activity, regulation, copy number and function in the glyoxalase system. *Biochem. Soc. Trans.* **42,** 419–424
19. Han, S., and Cohen, D. E. (2012) Functional characterization of thioesterase superfamily member 1/acyl-CoA thioesterase 11: implications for metabolic regulation. *J. Lipid Res.* **53,** 2620–2631
20. Marfori, M., Kobe, B., and Forwood, J. K. (2011) Ligand-induced conformational changes within a hexameric acyl-CoA thioesterase. *J. Biol. Chem.* **286,** 35643–35649
21. Emsley, P., and Cowtan, K. (2004) Coot: model-building tools for molecular graphics. *Acta Crystallogr. D Biol. Crystallogr.* **60,** 2126–2132
22. Adams, P. D., Afonine, P. V., Bunkóczi, G., Chen, V. B., Davis, I. W., Echols, N., Headd, J. J., Hung, L.-W., Kapral, G. J., Grosse-Kunstleve, R. W., McCoy, A. J., Moriarty, N. W., Oeffner, R., Read, R. J., Richardson, D. C., Richardson, J. S., Terwilliger, T. C., and Zwart, P. H. (2010) PHENIX: a

comprehensive Python-based system for macromolecular structure solution. *Acta Crystallogr. D Biol. Crystallogr.* **66,** 213–221
23. Leesong, M., Henderson, B. S., Gillig, J. R., Schwab, J. M., and Smith, J. L. (1996) Structure of a dehydratase-isomerase from the bacterial pathway for biosynthesis of unsaturated fatty acids: two catalytic activities in one active site. *Structure* **4,** 253–264
24. Dillon, S. C., and Bateman, A. (2004) The Hotdog-fold: wrapping up a superfamily of thioesterases and dehydratases. *BMC Bioinformatics* **5,** 109–109
25. Krissinel, E., and Henrick, K. (2007) Inference of macromolecular assemblies from crystalline state. *J. Mol. Biol.* **372,** 774–797
26. Khandokar, Y. B., Srivastava, P., Sarker, S., Swarbrick, C. M., Aragao, D., Cowieson, N., and Forwood, J. K. (2016) Structural and functional characterization of the PaaI thioesterase from *Streptococcus pneumoniae* reveals a dual specificity for phenylacetyl-CoA and medium-chain fatty acyl-CoAs and a novel CoA-induced fit mechanism. *J. Biol. Chem.* **291,** 1866–1876
27. Yamada, J., Furihata, T., Tamura, H., Watanabe, T., and Suga, T. (1996) Long-chain acyl-CoA hydrolase from rat brain cytosol: purification, characterization, and immunohistochemical localization. *Arch. Biochem. Biophys.* **326,** 106–114
28. Cantu, D. C., Chen, Y., and Reilly, P. J. (2010) Thioesterases: a new perspective based on their primary and tertiary structures. *Protein Sci.* **19,** 1281–1295
29. Forwood, J. K., Thakur, A. S., Guncar, G., Marfori, M., Mouradov, D., Meng, W., Robinson, J., Huber, T., Kellie, S., Martin, J. L., Hume, D. A., and Kobe, B. (2007) Structural basis for recruitment of tandem hotdog domains in acyl-CoA thioesterase 7 and its role in inflammation. *Proc. Natl. Acad. Sci. U.S.A.* **104,** 10382–10387
30. Jeong, J. H., Lee, K. H., Kim, Y. M., Kim, D. H., Oh, B. H., and Kim, Y. G. (2012) Crystal structure of the Gtr1p(GTP)-Gtr2p(GDP) protein complex reveals large structural rearrangements triggered by GTP-to-GDP conversion. *J. Biol. Chem.* **287,** 29648–29653
31. Battye, T. G., Kontogiannis, L., Johnson, O., Powell, H. R., and Leslie, A. G. (2011) iMOSFLM: a new graphical interface for diffraction-image processing with MOSFLM. *Acta Crystallogr. D Biol. Crystallogr.* **67,** 271–281
32. Petoukhov, M. V., Franke, D., Shkumatov, A. V., Tria, G., Kikhney, A. G., Gajda, M., Gorba, C., Mertens, H. D., Konarev, P. V., and Svergun, D. I. (2012) New developments in the ATSAS program package for small-angle scattering data analysis. *J. Appl. Crystallogr.* **45,** 342–350

Structural insights into GDP-mediated regulation of a bacterial acyl-CoA thioesterase

Yogesh B. Khandokar, Parul Srivastava, Nathan Cowieson, Subir Sarker, David Aragao, Shubagata Das, Kate M. Smith, Shane R. Raidal and Jade K. Forwood

J. Biol. Chem. 2017, 292:20461-20471.
doi: 10.1074/jbc.M117.800227 originally published online October 2, 2017
